Phys. Status Solidi A **207**, No. 2, 436–441 (2010) / **DOI** 10.1002/pssa.200925368

physica status solidi a
www.pss-a.com
applications and materials science

Simultaneous stress and defect luminescence study on silicon

Paul Gundel*, **Martin C. Schubert, and Wilhelm Warta**

Fraunhofer Institute for Solar Energy Systems (ISE), Heidenhofstr. 2, 79110 Freiburg, Germany

Received 16 July 2009, revised 14 September 2009, accepted 21 September 2009
Published online 30 October 2009

PACS 61.72.Hh, 72.20.Jv, 78.30.Am, 78.55.Ap

* Corresponding author: e-mail paul.gundel@ise.fraunhofer.de, Fax: +49 761 4588 9250

Internal stress is strongly correlated with the mechanical stability of silicon wafers and with the distribution of defects and thus the minority carrier lifetime, which is often the limiting parameter for multicrystalline (mc) silicon solar cells. Therefore, internal stress is a highly relevant parameter for mc silicon. In this paper, a qualitative internal stress measurement technique by photoluminescence spectroscopy for mc silicon is presented. This technique is based on the stress-induced-bandgap energy shift. Stress measurements are compared to defect luminescence images, which are gathered in the same measurement. The method is evaluated by stress measurements with micro-Raman spectroscopy.

1 Introduction The quality of multicrystalline (mc) silicon solar cells can be significantly reduced by internal stress. Internal stress reduces the mechanical stability of silicon wafers. Furthermore, stress is known to amplify the formation of dislocations and influence the distribution of impurities. Since dislocations and impurities are the limiting factors in mc silicon solar cells, a deeper knowledge about stress-related defects has high significance for photovoltaics. Stress in mc silicon was recently measured by micro-Raman spectroscopy by Becker et al. [1]. They demonstrated a sophisticated method to measure stress tensors and showed examples for the correlation between dislocation clusters and stress. In this paper, we demonstrate a qualitative stress measurement technique for mc silicon based on the stress dependence of the bandgap, which provides information about the minority carrier lifetime and the defect properties in the same measurement. In the last part the simultaneous stress and defect study is exemplified.

1.1 Stress-dependent bandgap energy The stress dependence of the bandgap energy was first reported in 1958 for hydrostatic stress [2] and in 1962 for uniaxial stress [3]. These experimental results were theoretically confirmed [4, 5]. Theory and experiment show that the stress dependence significantly differs for hydrostatic and uniaxial stress.

For hydrostatic stress P the indirect bandgap energy $E_{\Gamma-X}$ was determined in Refs. [2, 5] to be

$$E_{\Gamma-X} = E_0 - (14 \pm 1) \times 10^{-3} \frac{\text{meV}}{\text{MPa}} P \qquad (1)$$

with the bandgap energy E_0 at no applied pressure. This shift of the bandgap energy is caused by a shift of the degenerated X_1 and the $\Gamma_{25'}$ energies.

For uniaxial stress σ the bandgap energy does not only depend on the absolute stress value but also slightly on the stress direction in respect to the crystal orientation. Due to a split up of the X_1 and an energy shift of the X_1 and the $\Gamma_{25'}$ levels at uniaxial stress σ the minimum indirect bandgap energy $E_{\Gamma-X(\text{min})}$, which is determining the radiative recombination rate, is

$$E_{\Gamma-X} = E_0 - \alpha \times 10^{-3} \frac{\text{meV}}{\text{MPa}} \sigma \qquad (2)$$

with α being 93 (for uniaxial stress in the [100] direction), 90 ([111] direction) and 92 ([110] direction), respectively, as experimentally determined in Refs. [6, 7] with only little deviations. Theoretical values are stated in Ref. [5]. With changing bandgap energy also the peak of the band-to-band (BB) luminescence is shifted. This effect was shown to be in good agreement with theoretical values at 4.2 K for uniaxial

stress [8] and at room temperature for hydrostatic stress [9] in monocrystalline silicon wafers.

In this paper, we utilize this shift of the BB photoluminescence (PL) for the determination of the stress in mc silicon.

PL measurements can provide a scalar for stress but are unable to represent the tensor properties of stress, due to the fact, that no polarization dependence of the BB PL was reported in Ref. [10] and also could not be detected in this work. Therefore, we make some simplifying assumptions:

1. Since α in Eq. (2) varies only by up to 2% with varying direction and since PL cannot determine the crystal orientation, we assume an average value for α of 91.5 for our following calculations.
2. Since only stress close to the surface is measured and the wafer represents a nearly two-dimensional geometry, as in Ref. [1] plane stress can be assumed.
3. In addition uniaxial stress is assumed to be dominating throughout this paper and used for the calculation of stress. This limitation results in only qualitative stress measurements with PL spectroscopy. But since in many cases such as stress fields caused by crack tips uniaxial stress is indeed dominant [1], stress measurements based on the shift of the BB PL peak still provide valuable information on the internal stress of mc silicon.

These assumptions allow calculating the stress with Eq. (2) from the PL BB shift. We call this method Stress Mapping by Photoluminescence Spectroscopy (SMAPS).

At the same time PL spectroscopy offers the advantage of providing complementary material parameters within the same measurement with precise local alignment. By integrating the BB peak a qualitative measure for the minority carrier lifetime τ can be extracted, since the intensity of the BB peak is proportional to τ^2 [11] in the high injection level. Furthermore, dislocation PL can be detected and gives additional information about the minority carrier lifetime limiting defects [10, 12].

2 Experimental

2.1 PL spectroscopy The detection of stress in mc silicon by PL spectroscopy requires a high spatial and spectral resolution. The high spectral resolution is needed since the observed energy shifts for typical internal stress levels in mc silicon of about 40 MPa are lower than 1 meV. The high spatial resolution in the order of 1 μm is required, because the stress level in mc silicon can strongly shift over a few microns and a lower resolution leads to an averaging of the different stress levels. To meet these requirements we modified a commercial confocal Raman microscope for a good performance in the spectral region of interest. This resulted in a spatial resolution of slightly below 1 μm. This resolution was determined by measuring the distance between the two closest iron precipitates, which could be distinguished (see Ref. [13] for details on the detection of precipitates by PL spectroscopy). Due to the high injection level (according to our simulations up to $10^{18}\,\mathrm{cm}^{-3}$) the diffusion length of the excess carriers is limited by Auger recombination in combination with the high surface recombination velocity and therefore, does not limit the spatial resolution.

The generation laser is a 533 nm laser with a power of 17 mW on a spot with 0.9 μm diameter. For the mapping the sample is mounted on a motorized *XY* stage. The measurements in this paper use a 50× lens. The PL signal is split up by a $150\,\mathrm{g\,mm}^{-1}$ grating and detected by an InGaAs detector, thus for each measurement point a PL spectrum is recorded. Before the reflected laser beam reaches the grating it is suppressed by a filter. This setup provides a spatial resolution of 1 μm and a spectral resolution of 0.5 nm. The best results for detecting the stress-induced spectral shift were achieved by empirically fitting the BB PL with three overlapping Gaussian peaks, which have fixed amplitude ratios, fixed spectral distances and fixed spectral widths. The amplitude ratios and spectral widths and distances were determined by fitting three overlapping Gaussians to a representative spectrum, these parameters were not changed in the following fitting routine for the other spectra. The parameters, which were used here, are listed in Table 1.

In addition, a defect luminescence peak at 1250 nm (fixed position and spectral width) is included in the fit (see Fig. 5 for the spatial distribution of the defect luminescence intensity). This fitting routine results in three fitting parameters: (i) the amplitude, which is a measure for the minority carrier lifetime; (ii) the spectral position, which is a measure for stress, of the BB peak and (iii) the amplitude of the defect peak at 1250 nm. In this way a relative shift of the BB PL peak can be determined. The 95% confidence interval of the fit corresponds to an uncertainty of 0.8 MPa at each pixel. This uncertainty does not differ significantly for all spectra. A representative example for the fitting curve is shown in Fig. 1. The minority carrier lifetime does not influence the centre of the peak, since the PL intensity depends in the same way on τ for any wavelength of the BB peak, if reabsorption is neglected.

Table 1 The parameters, which were determined by fitting three Gaussians to a representative spectra. These parameters were used for determining the spatially resolved bandgap shift and are fixed during the fitting for the spatially resolved stress image.

fixed parameter	value
amplitude 1/amplitude 2	3.39
amplitude 1/amplitude 3	2.41
centre 2–centre 1	23.7 nm
centre 3–centre 1	64.9 nm
width 1	63.7 nm
width 2	21.4 nm
width 3	21.1 nm
defect centre	1240 nm
defect spectral width	90 nm

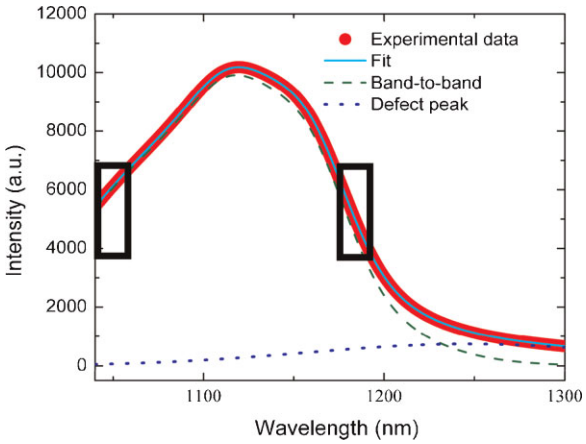

Figure 1 (online colour at: www.pss-a.com) Example for the fit with three Gaussian peaks for the BB PL with fixed amplitude ratios, fixed spectral distances and fixed spectral widths and an additional peak at 1240 nm for the dislocation luminescence. The fit consists of the band-to-band and the defect luminescence, which are shown separately. The error for the position of the BB PL corresponds to an uncertainty of the stress of 0.8 MPa for each pixel. The rectangles are the details, which are shown in Fig. 2. The experimental data is from the measurement, which was also used for Fig. 4.

From the energy shift of the BB PL the stress levels can be calculated with Eq. (2). To correct this image for the drift of the grating a fast Fourier transformation (FFT) correction is applied, which suppresses the effect of a slowly drifting grating by a high frequency pass filter. Details of a spectrum at tensile and of a spectrum at compressive stress are shown in Fig. 2, which demonstrates the relative spectral shift of the spectra.

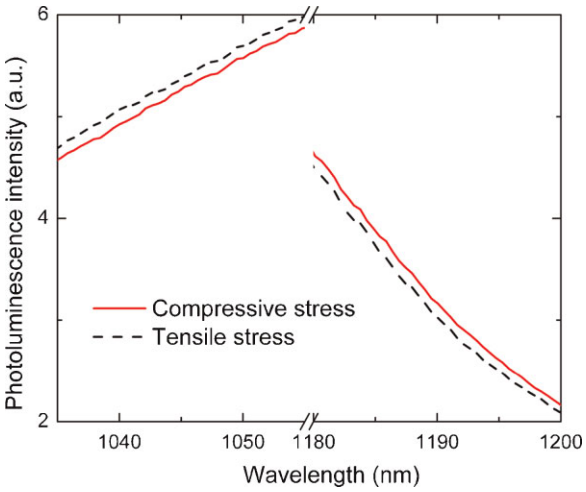

Figure 2 (online colour at: www.pss-a.com) Details of two normalized spectra for an area with compressive and an area with tensile stress are shown to demonstrate the relative shift of the spectra. The lines are moving averages over 5 points for an easier comparison. The positions of theses details are marked in Fig. 1.

2.2 Raman spectroscopy For the evaluation of SMAPS the microscope also allows basic micro-Raman spectroscopy. For this the same objective and laser, a 1800 g mm^{-1} grating and a silicon detector are used. The recorded Raman spectra were analysed as described in Ref. [14]: A Lorentz function is fitted to the first order Raman peak, which is located at about 521 cm^{-1} (for Raman spectroscopy the energy is usually stated relative to the incident wavelength in reciprocal wavelengths). For the correction for shifts of the grating the Rayleigh peak position of the laser is subtracted from the position of the first order Raman peak. As additional correction an FFT correction is applied, which reduces the effect of instabilities of the detector. From the shift $\Delta\omega$ of the peak the relative stress level $\Delta\sigma$ can be calculated by the equation for uniaxial stress [14], which is assumed to be dominating in this paper

$$\Delta\sigma = 500\,\frac{\text{MPa}}{\text{cm}^{-1}}\,\Delta\omega. \tag{3}$$

Since the Raman spectrum depends on the grain orientation, the laser's and its own polarization, nearly all components of stress tensors can be calculated [1].

2.3 Low temperature PL As further comparison and to clarify the origin of the observed energy shift, SMAPS is repeated at 80 K, which excludes possible defect luminescence peaks close to the BB peak as an alternative origin of the energy shift, since the defect peaks are clearly separated from the BB PL at 80 K. Two representative BB PL peaks at different stress levels at 80 K are shown in Fig. 3. The shift at different stress levels is clearly visible.

3 Results

3.1 SMAPS at room temperature For the evaluation of SMAPS we measured the spatially resolved PL spectra of a standard industrial mc silicon wafer from the

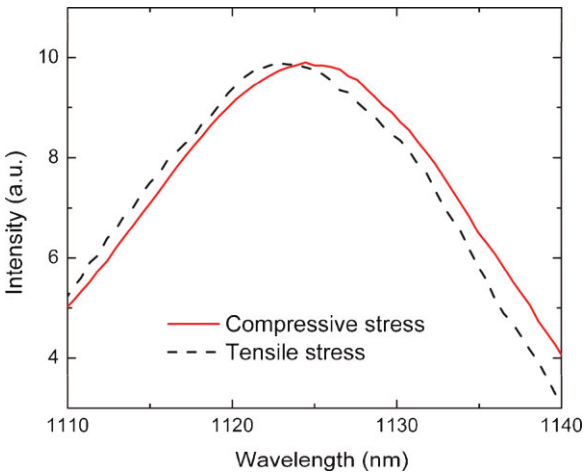

Figure 3 (online colour at: www.pss-a.com) Two representative spectra of the BB PL at 80 K. The shift of the peak is clearly visible. The lines are moving averages over 5 measurement points.

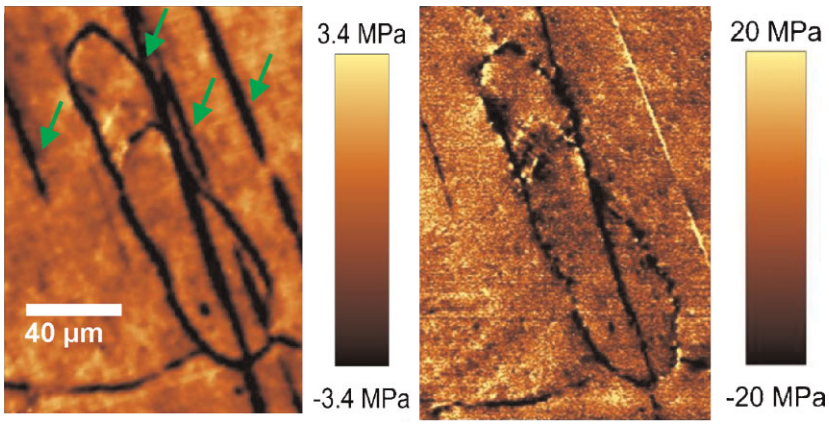

Figure 4 (online colour at: www.pss-a.com) The comparison of the stress calculated from a PL measurement on the left-hand side and the stress calculated from a Raman measurement on the right-hand side shows qualitative agreement between both measurements. The straight lines are scratches from the polishing on the front side (arrows). The Raman determined stress is by a factor 6 higher than the PL determined stress.

middle of an ingot. This $10^{16}\,cm^{-3}$ boron doped wafer was polished and the surface was left unpassivated. Due to the resulting high surface recombination velocity of about $10^5\,cm\,s^{-1}$ [15] the effective τ is limited to 5 µs. Therefore the PL intensity, which is proportional to τ^2, is rather small. An integration time of 4 s per pixel was sufficient to get an image of the frequency shift (see Fig. 4 on the left). For the PL spectroscopy three pixels were measured for each 2 µm. For the Raman spectroscopy two pixels per µm were measured with an integration time of 0.07 s for each pixel. In Fig. 4 SMAPS is compared to the stress, which is calculated from the Raman measurement without a specific orientation setting. The average of all pixels is taken as 0-stress level in all cases.

This comparison reveals that both measurements are in good qualitative agreement. But the stress is by a factor 6 higher for the Raman results. This deviation might have several reasons:

1. The stress measurement with Raman only detects photons up to a depth of about 1 µm (absorption length of 533 nm in silicon is 0.95 µm), whereas the depths of SMAPS is mainly restricted by the confocal setup (absorption length of 1100 nm in silicon is about 150 µm), which has a depth of focus of about 3 µm. This integration over 3 µm depth averages over different stress levels; this has the potential to systematically reduce the absolute PL measured stress.
2. The spatial resolution of SMAPS is lower, since the aberration of the optical elements is higher between the 533 nm excitation laser and the detected signal around 1100 nm than for the Raman spectroscopy, where the excitation wavelength and the detected signal virtually have the same wavelength. In addition the diffraction limit of SMAPS is double the size as of the Raman spectroscopy. The lower resolution for PL leads to an averaging over different stress levels, which reduces the measured stress.
3. Deviations from the assumption of uniaxial stress can lead to different results for both techniques due to the polarization dependence of the Raman signal and the dependence of the bandgap energy shift on the stress symmetry.
4. Defect peaks close to the BB PL, which make a determination of the spectral shift difficult.

3.2 Impact of spatial resolution In order to test the impact of the first two effects the depth of focus was increased to approximately 4.5 µm and the spatial resolution to 3 µm by enlarging the size of the pinhole in front of the detection system. This decreases the required integration

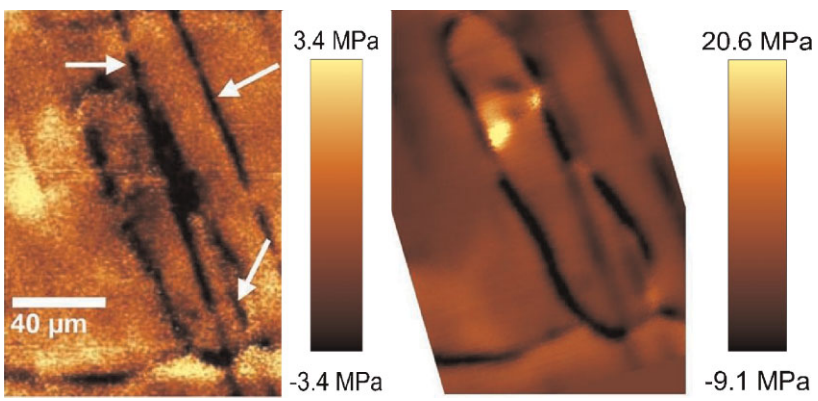

Figure 5 (online colour at: www.pss-a.com) On the left-hand side the result for the depth of focus of the microscope of about 4.5 µm is shown. The qualitative agreement with the Raman measurement (Fig. 4) is worsened due to the lower spatial resolution and there is still a factor 6 difference between the Raman and the PL results. On the right-hand side the stress measured by PL at 80 K is shown. The stress is in good quantitative agreement with the Raman measurement in Fig. 4. The arrows mark surface scratches, which result in strong deviations of SMAPS from Raman due to optical effects.

time to 0.1 s for each pixel because the total signal is higher. The SMAPS result with lower spatial resolution is shown in Fig. 5.

Even though the spatial resolution and depth of focus was changed, there is still a difference of a factor 6 between the Raman and the PL results. Since this factor is approximately independent of spatial resolution and depth of focus, the deviation is most likely due to the over-simplifying assumption of uniaxial stress.

3.3 SMAPS at 80 K By cooling the sample to 80 K the BB PL peak is narrowed and thereby the noise level reduced; additionally possibly existing defect PL close to the BB PL are clearly separated from the BB PL. Therefore, cooling is a test to verify the origin of the BB PL shift.

The stress calculated from the shift of the peak at 80 K is shown in Fig. 4 on the right-hand side. The shift is extracted by a fit with three Gaussian peaks with fixed amplitude ratios and fixed spectral distances, leaving two fitting parameters: the amplitude and the spectral position. The error of the fit leads to an uncertainty in the stress level of 0.7 MPa. The pinhole with a depth of focus of 4.5 μm and an integration time of 0.1 s is applied for this measurement. Balslev [6] showed that at 80 K the bandgap depends on stress virtually in the same way as at 295 K. Therefore, the stress is calculated by formula (2). This measurement leads to a reasonable quantitative agreement between SMAPS at 80 K and the Raman measurement, but the spatial resolution is significantly lower. This suggests, that either defect luminescence close to the BB PL or the broadness of the BB PL peak and the resulting noise at 300 K in the shift determination is reducing the detectable shift and thus the calculated stress at room temperature. The SMAPS maps in Figs. 4 and 5 (left-hand side) suggest that this effect decreases the calculated absolute stress systematically. For a possible empirical correction of this effect by multiplying the result with a constant factor a broader experimental basis is required.

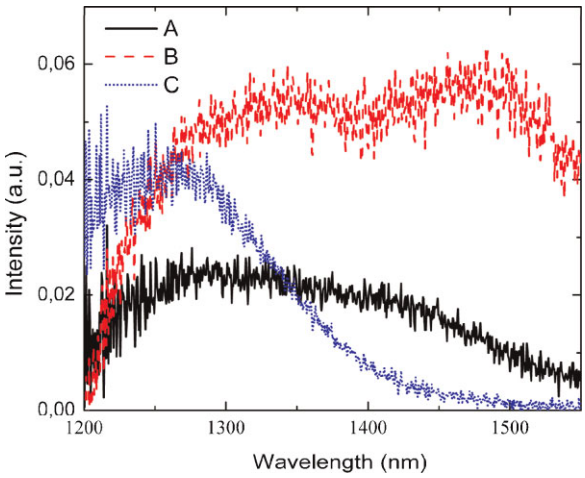

Figure 6 (online colour at: www.pss-a.com) Typical defect spectra, which were recorded simultaneously with the SMAPS measurement in Fig. 4 at room temperature. The spectra are normalized to the BB PL maximum and a representative PL spectrum without defect PL was subtracted in order to make defect PL close to the BB PL visible. Spectrum A is a spectrum with defect luminescence at 1250 nm (0.99 eV) and 1330 nm (0.93 eV), spectrum B shows luminescence at 1330 nm (0.93 eV) and 1500 nm (0.83 eV) and spectrum C shows only luminescence at 1250 nm (0.99 eV).

3.4 Defect spectroscopy and lifetime In the following the simultaneous gathering of complementary material parameters, which allows directly correlating these parameters with stress, is exemplified. This represents the advantage of SMAPS. Three representative defect spectra at room temperature recorded simultaneously with the SMAPS measurement in Fig. 4 are depicted in Fig. 6. For making the defect PL in the spectral vicinity of the BB PL visible the spectra were normalized with the BB PL maximum and a representative spectrum without defect PL was subtracted.

The qualitatively determined lifetime image and the defect luminescence images, which were taken at room temperature in the same measurement with the SMAPS image in Fig. 4 on the left, are shown in Fig. 7.

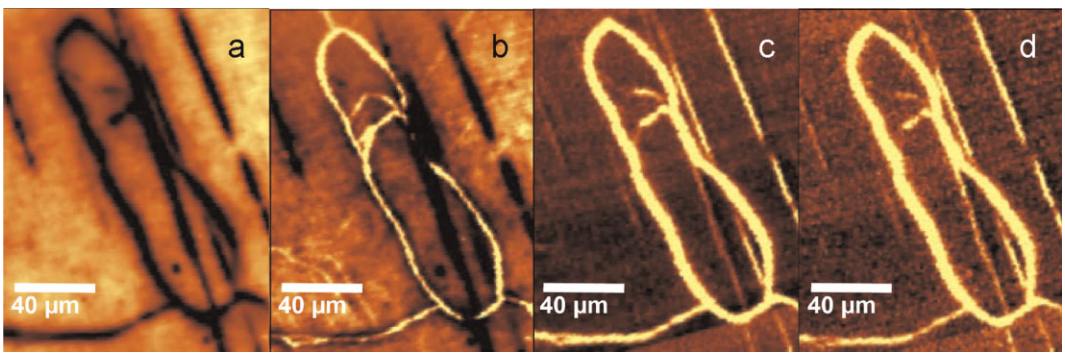

Figure 7 (online colour at: www.pss-a.com) Images of the qualitative lifetime (a) and the defect PL (b–d) taken simultaneously with the stress image of Fig. 4 in one measurement at room temperature. The image of the qualitative minority carrier lifetime is depicted in (a) (bright means high lifetime), (b) shows the amplitude of the fitted Gaussian peak at 1250 nm (peak at 0.99 eV), (c) the integrated intensity between 0.92 and 0.94 eV (peak at 0.93 eV) and (d) the integrated intensity between 0.81 and 0.84 eV (peak at 0.83 eV) (bright means high intensity for all defect luminescence images).

Figure 7 shows a strongly reduced lifetime and an increased defect luminescence in areas of high stress. It is well known that crystal defects (dislocations, grain boundaries) and precipitates cause internal stress [1]. In Ref. [1] dislocations were also shown to form at grain boundaries during the solidification process in order to relief stress. On the other hand crystal defects are known to limit the minority carrier lifetime, in particular if they are decorated by transition metals [16]. Thus, the strong correlation between low lifetime and high stress is expected.

Defect PL can give additional information on the energy levels of the involved defects. So far defect PL with an energy peak of approximately 0.8 eV has been reported at 300 K and was attributed to dislocations or oxygen defects [10, 17, 18]. We found two more defect lines with peak energies of 0.93 and 0.99 eV. The similarity between these two images and their energy difference of about 60 meV suggest that the 0.93 eV PL is a phonon replica of the 0.99 eV PL. The energy positions suggest, that these two peaks are the same as the so-called D3 and D4 lines, which have been only reported below 100 K so far and were attributed to dislocations [19]. The defect PL correlates to the areas of high stress, which suggests a common origin of stress and this defect PL.

The described effects have also been detected on surface passivated samples and solar cells. For these samples the required integration time is smaller due to the increased PL intensity because of the lower surface recombination.

4 Conclusion We proved the feasibility of qualitative stress measurements in mc silicon by PL spectroscopy. The advantage of this method, the simultaneous measurement of the minority carrier lifetime and the defect luminescence, is demonstrated for an example, where a correlation between stress, lifetime and defect PL is shown. The difference in the absolute stress level of PL measurements compared to Raman measurements probably arises from the oversimplifying assumption of uniaxial stress. While SMAPS is helpful to investigate correlations between defect luminescence, minority carrier lifetime and stress, the clear advantage of the Raman stress measurements is the quantitative measurability of full stress tensors.

Acknowledgements We would like to thank Tobias Kalden for the sample preparation, Michael Becker from the Max-Planck-Institute for Microstructure Physics and Martin Kasemann for fruitful discussions. This research was funded by the German BMU in the SolarFocus project (0327650H).

References

[1] M. Becker, H. Scheel, S. Christiansen, and H. P. Strunk, J. Appl. Phys. **101**, 063531 (2007).
[2] W. Paul and D. M. Warschauer, J. Phys. Chem. Solids **5**, 89 (1958).
[3] W. Rindner, J. Appl. Phys. **33**, 2479 (1962).
[4] I. Goroff and L. Kleinman, Phys. Rev. **132**, 1080–1084 (1963).
[5] J. J. Wortman, J. R. Hauser, and R. M. Burger, J. Appl. Phys. **35**(7), 2122 (1964).
[6] I. Balslev, Phys. Rev. **143**, 636 (1966).
[7] L. D. Laude, F. H. Pollak, and M. Cardona, Phys. Rev. B **3**, 2623 (1971).
[8] K. Yasutake, M. Umeno, H. Kawabe, H. Nakayama, T. Nishino, and Y. Hamakawa, Jpn. J. Appl. Phys. **21**(12), 1715 (1982).
[9] Y. Ishibashi, T. Kobayashi, A. D. Prins, J. Nakahara, M. A. Lourenco, R. M. Gwilliam, and K. P. Homewood, Phys. Status Solidi B **244**(1), 402 (2007).
[10] S. Ostapenko, I. Tarasov, J. P. Kalejs, C. Haessler, and E.-U. Reisner, Semicond. Sci. Technol. **15**, 840 (2000).
[11] P. Würfel, J. Phys. C **15**, 3967 (1982).
[12] M. Suezawa and K. Sumino, Phys. Status Solidi A **78**, 639 (1983).
[13] P. Gundel, M. C. Schubert, W. Kwapil, J. Schön, M. Reiche, H. Savin, M. Yli-Koski, J. A. Sans, G. Martinez-Criado, W. Seifert, W. Warta, and E. R. Weber, Phys. Status Solidi RRL **3**, 230 (2009).
[14] I. De Wolf, Semicond. Sci. Technol. **11**, 139 (1996).
[15] A. A. Istratov, H. Hieslmair, and E. R. Weber, Appl. Phys. A: Mater. Sci. Process. A **70**, 489 (2000).
[16] M. Seibt, R. Khalil, V. Kveder, and W. Schröter, Appl. Phys. A **96**, 235 (2009).
[17] E. Ö. Sveinbjörnsson and J. Weber, Appl. Phys. Lett. **69**, 2686 (1996).
[18] V. Kveder, M. Badylevich, E. Steinman, A. Izotov, M. Seibt, and W. Schröter, Appl. Phys. Lett. **84**, 2106 (2004).
[19] R. Sauer, J. Weber, J. Stolz, E. R. Weber, K. H. Küsters, and H. Alexander, Appl. Phys. A **16**(1), 1 (1985).